EPJ Web of Conferences **371**, 01009 (2026) https://doi.org/10.1051/epjconf/202637101009
*AMT'2026*

# Mixed Convection and Surface Radiation in an Inclined Ventilated Cavity under Injection and Suction Modes

*Khadija* Ezzaraa[1]*, *Ahmed* Bahlaoui[1], *Ismail* Arroub[1], *Abdelghani* Raji[2] and *Mohammed* Hasnaoui[3]

[1]Research Laboratory in Physics and Sciences for Engineers (LRPSI), Polydisciplinary Faculty, B. P. 592, Béni-Mellal, Morocco
[2]Energy and Materials Engineering Laboratory (LGEM), Faculty of Sciences and Technics, B. P. 523, Béni-Mellal, Morocco
[3]Laboratory of Fluid Mechanics and Energetics (LMFE), Faculty of Sciences Semlalia, B. P. 2390, Marrakech, Morocco

**Abstract.** A numerical study of mixed convection coupled with surface radiation in an inclined ventilated rectangular cavity is presented. Air is used as the working medium, and a uniform heat flux is imposed on the active wall, while the remaining walls are adiabatic; all boundaries are considered radiatively participating. The analysis examines the coupled effects of wall emissivity, inclination angle and ventilation mode (injection versus suction) on the flow pattern and thermal performance, quantified through convective, radiative, and total Nusselt numbers, as well as mean and maximum temperatures. The results show that cavity inclination significantly modifies recirculation patterns, leading to noticeable variations in convective heat transfer. Increasing wall emissivity from $\varepsilon$ = 0.15 to 0.85 enhances the total heat transfer by approximately 26–30%, while the radiative contribution reaches ≈ 40%., with the average total Nusselt number increasing by up to ≈ 7% when switching from suction to injection mode Radiation also induces a marked reduction in both mean temperature and maximum wall temperature, with peak temperatures becoming nearly insensitive to inclination at high emissivity. The radiative contribution remains significant over the entire range of studied parameters and cannot be neglected, even for low emissivity values. It is slightly more pronounced in suction mode, whereas injection generally provides more effective overall cooling and lower maximum temperatures.

## 1 Introduction

Efficient thermal management is essential in many engineering applications where high power densities and compact geometries lead to significant heat generation and an increased risk of overheating. Ventilated cavities are widely employed as simple and effective cooling configurations, particularly in electronics cooling, solar thermal systems,

* Corresponding author: ezzaraakhadija@gmail.com

passive building applications, and compact heat exchangers. In such systems, heat transfer is governed by mixed convection, resulting from the interaction between buoyancy-induced natural convection and externally imposed forced flow. This behaviour can be strongly altered when the confining walls participate in surface radiation, which significantly modifies the temperature distribution and overall thermal performance. Moreover, tilting the enclosure changes the orientation of the gravitational acceleration relative to the main flow direction, which can profoundly reorganise the flow structure, potentially transforming a single recirculation cell into more complex multi-vortex patterns. A comprehensive understanding of the combined effects of inclination angle, surface radiation, and ventilation configuration is therefore essential for the design and optimisation of thermally efficient systems.

Considerable attention has been given to natural convection–radiation coupling in enclosed cavities [1–4], particularly with respect to the role of geometrical parameters. These studies demonstrated that surface radiation can substantially modify the thermal field by promoting a more uniform temperature distribution and reducing thermal gradients inside the enclosure. Moreover, radiative exchange contributes to the improvement of global heat transfer, mainly through its effect on the mean Nusselt number and the overall thermal performance. For mixed convection combined with surface radiation, many numerical and experimental studies have also been reported under different boundary conditions. Daiz et al. [5] used the lattice Boltzmann method to analyze radiative mixed convection in a discretely heated square lid-driven cavity. Their results revealed the presence of a dominant recirculation cell generated by the combined action of shear-driven flow and buoyancy forces. They also showed that increasing wall emissivity strengthens the radiative and total heat transfer rates, while reducing the convective contribution. However, increasing the Richardson number led to a clear decrease in both convective and overall heat transfer, with only a slight enhancement of the radiative component. Hidki et al. [6] numerically investigated radiative mixed convection in a ventilated horizontal channel containing finned heat-generating cylinders. Their findings indicated that increasing the Reynolds number and wall emissivity improves the thermal performance. Without radiation, straight and curved fins were found to reduce the maximum temperature by about 6.6 °C. Whereas when radiation was considered, straight fins provided superior cooling efficiency. Ganesan et al. [7] examined coupled convection–radiation heat transfer in horizontal square ducts subjected to various heating configurations. Their results showed that surface radiation has a significant influence on the overall heat transfer, even at relatively low temperatures. The total Nusselt number was strongly affected by the Reynolds number, wall emissivity, heating orientation, temperature distribution, and flow structure inside the duct. Using the Lattice Boltzmann method, Dahani et al. [8] investigated mixed convection with surface radiation in a square lid-driven cavity subjected to spatially sinusoidal thermal boundary conditions. Their findings showed that the Richardson number strongly affects the hydrodynamic field and heat transfer behavior, and that the radiative contribution remains significant even at low Richardson numbers, increasing further as this parameter rises. Prakash and Singh examined, through both experimental measurements [9] and numerical simulations [10], steady laminar mixed convection coupled with surface radiation in an air-filled ventilated cavity. Covering wide ranges of Reynolds and Richardson numbers, their results demonstrated that surface radiation has a strong influence on both the Nusselt number and the maximum wall temperature. Based on experimental data, empirical correlations were developed to support practical thermal design. Raji and Hasnaoui [11] numerically examined mixed convection and radiation in a ventilated rectangular enclosure with varying inlet/outlet configurations. Their findings indicated that surface radiation promotes a more uniform temperature distribution. For the bottom-to-top ventilation arrangement, radiation tends to raise the average temperature inside the cavity while

reducing the peak temperature. In contrast, under the top-to-bottom configuration, both the average and maximum temperatures are reduced. Bahlaoui et al. [12] extended this work to partitioned ventilated cavities, demonstrating that the relative height of an adiabatic partition increases radiative heat transfer while reducing the convective component at the heated wall.

Overall, these investigations clearly demonstrate that surface radiation is far from negligible and can substantially modify the thermal behaviour of both closed and ventilated cavities. Although radiative effects may be weak in systems with small temperature differences or low emissivity surfaces, such conditions are rarely encountered in practical applications. Consequently, the present work investigates the interaction between mixed convection and surface radiation in an inclined ventilated cavity, with particular emphasis on the combined effects of cavity inclination, wall emissivity, and ventilation configuration on flow structure, temperature distribution, and overall heat-transfer performance.

## 2 Problem formulation

The physical configuration considered in this work is illustrated in Figure 1. It consists of a rectangular vented enclosure characterized by an aspect ratio A = 2. A uniform heat flux is imposed on the left vertical wall, whereas the remaining walls are assumed to be perfectly adiabatic. The working fluid is air, modeled as a Newtonian fluid, and is driven through the cavity by two openings located at mid-height on the lateral walls. Two ventilation arrangements are considered: injection mode, shown in Fig. 1a, and suction mode, shown in Fig. 1b. The cavity walls are assumed to be grey and diffuse radiative surfaces with constant emissivity, allowing both emission and reflection of thermal radiation. The flow is considered laminar and two-dimensional, and buoyancy effects are taken into account using the Boussinesq approximation. Based on the adopted assumptions, the nondimensional equations describing mass, momentum, and energy conservation are expressed using the vorticity–stream function formulation as follows:

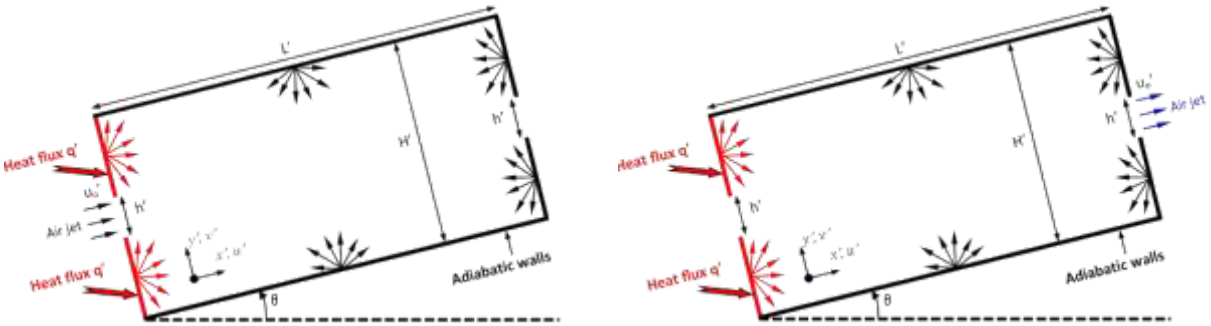


a) Injection mode b) Suction mode

**Fig. 1.** Schematic illustration of the investigated configuration

$$\frac{\partial \Omega}{\partial t} + u\frac{\partial \Omega}{\partial x} + v\frac{\partial \Omega}{\partial y} = \frac{Ra}{Re^2 Pr}\left[\cos\theta\frac{\partial T}{\partial x} - \sin\theta\frac{\partial T}{\partial y}\right] + \frac{1}{Re}\left(\frac{\partial^2 \Omega}{\partial x^2} + \frac{\partial^2 \Omega}{\partial y^2}\right) \quad (1)$$

$$\frac{\partial T}{\partial t} + u\frac{\partial T}{\partial x} + v\frac{\partial T}{\partial y} = \frac{1}{RePr}\left(\frac{\partial^2 T}{\partial x^2} + \frac{\partial^2 T}{\partial y^2}\right) \quad (2)$$

$$\frac{\partial^2 \Psi}{\partial x^2} + \frac{\partial^2 \Psi}{\partial y^2} = -\Omega \quad (3)$$

The velocity components can be expressed in terms of the stream function and vorticity using the following relations:

$$u = \frac{\partial \Psi}{\partial y}\ ,\ v = -\frac{\partial \Psi}{\partial x} \text{ and } \Omega = \frac{\partial v}{\partial x} - \frac{\partial u}{\partial y} \quad (4)$$

### 2.1 Imposed Boundary Conditions

For both injection and suction configurations, the nondimensional boundary conditions imposed on the computational domain are defined as follows:

| | |
|---|---|
| $u = v = 0$ | at the solid boundaries |
| $T = 0$ | at the inlet opening |
| $\Psi = B$ | on the walls above the opening ports |
| $\Psi = 0$ | on the walls under the opening ports |
| $-\frac{\partial T}{\partial x} + N_r Q_r = 1$ | along the hot vertical wall |
| $-\frac{\partial T}{\partial n} + N_r Q_r = 0$ | at the thermally insulated walls |

″n″ denotes the outward normal direction to the wall under consideration.

*Injection case*:

$v = \Omega = 0$, $u = 1$ and $\psi = y - \frac{(1-B)}{2}$ at the inlet boundary

For the injection configuration, the boundary conditions at the outlet opening are not prescribed explicitly. Therefore, the variables u, v, T, Ψ and Ω are extrapolated at each time step using a zero second-order normal derivative condition at the outlet.

*Suction case*:

$v = \Omega = 0$, $u = 1$ and $\psi = y - \frac{(1-B)}{2}$ at the outlet boundary

In the suction configuration, the hydrodynamic variables for u, v, Ψ and Ω are not prescribed at the inlet boundary, while the temperature T is unknown at the outlet. These quantities are updated at each time step using a zero second-order normal derivative condition at the corresponding opening.

The boundary conditions at the cavity outlet in injection mode and at the inlet in suction mode are not known a priori. In open systems, various boundary conditions have been proposed in the literature, including incompressibility-based conditions and fully developed flow assumptions. However, such approaches are not appropriate when the flow at the outlet or inlet exhibits reversed-flow structures. Consequently, a non-restrictive and more realistic numerical treatment is adopted. For both injection and suction modes, the temperature T, stream function Ψ, vorticity Ω, and velocity components u and v are extrapolated at the corresponding open boundaries (outlet for injection and inlet for suction) by imposing zero second-order derivatives in the direction normal to the boundary.

Since no explicit physical boundary condition is available for vorticity at solid walls, Woods' approximation [13] is adopted.

$$\Omega_{\omega} = -\frac{1}{2}\Omega_{\omega+1} - \frac{3}{\Delta\eta^2}(\Psi_{\omega+1} - \Psi_{\omega}) \tag{5}$$

In the above equation, the subscript ω indicates the wall, while Δη denotes the grid spacing along the outward normal direction to the wall.

### 2.2 Radiation Equations

To evaluate the radiative heat exchange between the cavity walls and their surroundings, an enclosure analysis based on the net-radiation method is adopted. In this framework, the radiosity of each wall element is computed. The cavity boundaries are discretised into N = 604 elements, consistent with the computational grid (201×101), and each element is assumed isothermal owing to its small size. The view factors between these isothermal surfaces are determined using Hottel's crossed-string technique [14]. The inlet and outlet openings are modelled as black surfaces maintained at the ambient temperature. Assuming that the air inside the enclosure does not participate in radiative heat transfer, the dimensionless radiosity relation for the $i^{th}$ surface element is given by:

$$J_i = \varepsilon_i \left(\frac{T_i}{T_o} + 1\right)^4 + (1 - \varepsilon_i) \sum_{j=1}^{N} F_{ij} J_j \tag{6}$$

For each discrete surface "$S_i$", the dimensionless net radiative heat flux is evaluated as follows:

$$Q_r = J_i - I_i = \varepsilon_i \left[ (\frac{T_i}{T_o} + 1)^4 - \sum_{j=1}^{N} F_{ij} J_j \right] \tag{7}$$

### 2.3 Heat Transfer

The knowledge of the heat transfer rate exchanged between the system under study and its environment is provided by the calculation of the Nusselt number. The average convective and radiative Nusselt numbers on the heated wall are obtained as follows:

$$\begin{aligned} Nu_H(cv) &= \frac{2}{1-B}\left( - \int_0^{0.5-\frac{B}{2}} \frac{1}{T}\left(\frac{\partial T}{\partial x}\right)\Big|_{x=0} dy - \int_{0.5+\frac{B}{2}}^{1} \frac{1}{T}\left(\frac{\partial T}{\partial x}\right)\Big|_{x=0} dy \right); \\ Nu_H(rd) &= \frac{2}{1-B}\left( \int_0^{0.5-\frac{B}{2}} \frac{1}{T}(N_r Q_r)|_{x=0} dy + \int_{0.5+\frac{B}{2}}^{1} \frac{1}{T}(N_r Q_r)|_{x=0} dy \right) \end{aligned} \tag{8}$$

The total Nusselt number, $Nu_H$, as the sum of the corresponding convective and radiative Nusselt numbers; i.e. $Nu_H = Nu_H(cv) + Nu_H(rd)$.

### 2.4 Numerics

Eqs. (1)–(3) are solved by means of a finite-difference numerical scheme. Central approximations are employed for the diffusion terms, including both first- and second-order derivatives, while a second-order upwind treatment is used for the advective terms to reduce possible numerical oscillations in the mixed convection regime. The ADI algorithm is adopted for advancing Eqs. (1) and (2) in time. For each time level, the stream-function Poisson equation, Eq. (3), is resolved using the PSOR method, where an optimal over-

relaxation coefficient of 1.88 is retained for the chosen mesh. Finally, the set of algebraic equations describing surface radiative exchange, Eq. (6), is handled iteratively using the Gauss–Seidel procedure.

### 2.5 Grid Independence Analysis and Numerical Code Validation

To assess the accuracy of the numerical procedure, the developed code was first validated against the classical benchmark of natural convection coupled with radiation in a differentially heated square cavity. The average Nusselt number at the heated wall was compared with the results of Wang et al. [15], and very good agreement was obtained, with a maximum relative deviation not exceeding 1.62% (Figure 2). In a second step, a grid sensitivity study was carried out by solving the problem on several uniform meshes. The effect of grid refinement was evaluated using the total average Nusselt number and the maximum stream function value at the heated wall. The results show that a 201×101 grid provides sufficient accuracy for the present configuration, since further refinement to a 281×141 mesh leads to variations of less than 0.86 % and 1.37 % for $\Psi_{max}$ and $Nu_H$ respectively.

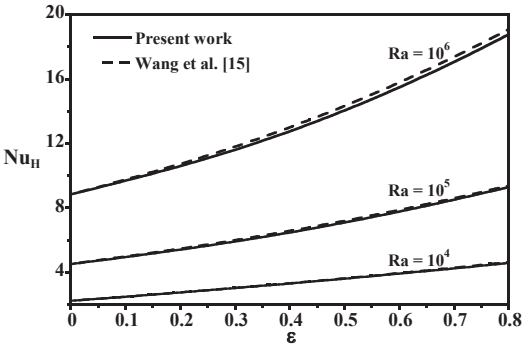


**Fig. 2.** Influence of surface emissivity and the Rayleigh number on the average total Nusselt number, $Nu_H$, along the hot wall of a differentially heated square cavity, with $T'_H$ = 298.5 K and $T'_C$ = 288.5 K.

## 3 Results and discussion

The inclination angle of the cavity strongly affects mixed convection heat transfer by modifying the relative orientation of buoyancy and forced flow, so that natural convection may either assist or oppose the imposed injection or suction. This interaction governs the flow structure and thermal behavior and is further altered when surface radiation is considered. In this study, the Rayleigh number Ra, the convection–radiation interaction parameter Nr, and the reference dimensionless temperature $T_0$ are the main controlling parameters and cannot be varied independently. In the present study, the inlet temperature is fixed at $T_F'$=298.15 K and the Rayleigh number at Ra=$10^6$, yielding $N_r$=3.52 and $T_0$=10.1. The effects of cavity inclination θ, wall emissivity ε, and ventilation mode (injection or suction) are examined using air as the working fluid (Pr=0.72), with a constant opening height ratio h=1/5.

The impact of cavity inclination on thermal and hydrodynamic fields and under injection mode were illustrated in Figure 3. The simulations were conducted for a moderate wall emissivity (ε = 0.5), a Reynolds number of Re = 300, and inclination angles varying from 0° (left side heating) to 90° (bottom heating). At θ = 0° (Figure 3a), corresponding to a horizontal cavity heated on the left vertical wall, the hydrodynamic field is characterized by a large clockwise recirculation cell that develops in the lower region of the cavity, beneath

the primary imposed flow. This cell results from the combined effects of viscous shear and buoyancy-driven convection. Two small secondary vortices appear in the upper corners. The isotherms are tightly packed near the heated wall, indicating strong thermal gradients and thus intense heat transfer. Additionally, radiation effects generate a global thermal gradient extending across the cavity from the insulated surfaces. As the cavity inclination increases from 30° to 90° (Figures 3b–3e), the flow and temperature fields undergo notable changes. The reorientation of gravity relative to the forced flow modifies the buoyancy contribution, leading to a progressive reduction and eventual disappearance of both the main lower cell and the secondary vortices and to the dominance of open forced-convection streamlines. At θ = 90° (Figure 3e), the cavity, now heated from below, exhibits a nearly symmetric flow and temperature field, with a cold central zone separating the hot lower region from the cooler upper part, highlight the role of buoyancy at high inclination angles and its interaction with surface radiation and forced flow.

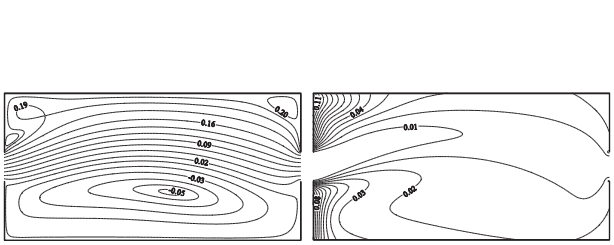

**a)** θ = 0° ($\Psi_{min}$ = -0.048, $\Psi_{max}$ = 0.201)

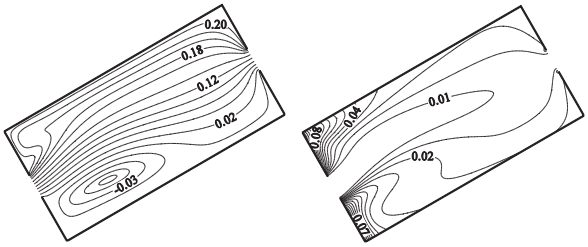

**b)** θ = 30° ($\Psi_{min}$ = -0.035., $\Psi_{max}$ = 0.201

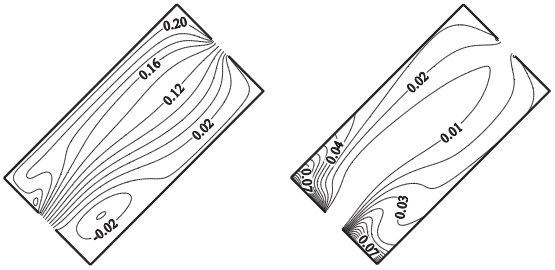

**c)** θ = 45° ($\Psi_{min}$ = -0.029., $\Psi_{max}$ = 0.201)

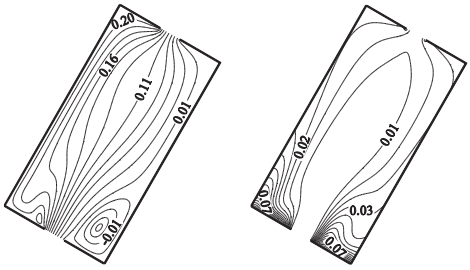

**d)** θ = 60° ($\Psi_{min}$ = -0.022, $\Psi_{max}$ = 0.201)

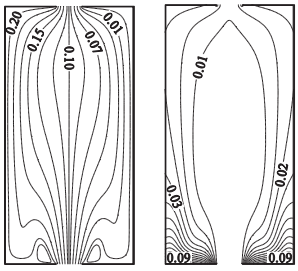

**e)** θ = 90° ($\Psi_{min}$ = -0.002, $\Psi_{max}$ = 0.202)

**Fig. 3.** Flow and thermal fields, in the injection mode, for ε = 0.5, Re = 300 and different cavity inclinations

In the suction mode (Figure 4(a–e)), for θ = 0°, the overall flow pattern is similar to that observed in injection mode, except near the upper left corner, where the recirculating cells are larger and more intense due to the absence of jet impingement that would otherwise weaken or remove them. When θ increases from 30° to 90°, the flow and thermal fields undergo changes qualitatively similar to those reported for the injection mode. However, the cold central zone that develops with inclination remains comparatively thinner in suction mode, implying thicker thermal boundary layers and thus slightly weaker heat transfer. This observation suggests that, from a thermal point of view, the injection configuration is more efficient than the suction one.

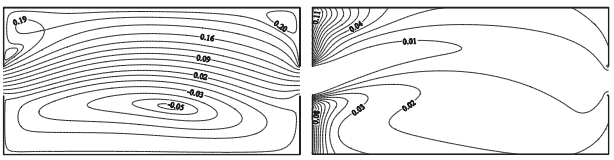

**a)** θ = 0° ($\Psi_{min}$ = -0.059, $\Psi_{max}$ = 0.204)

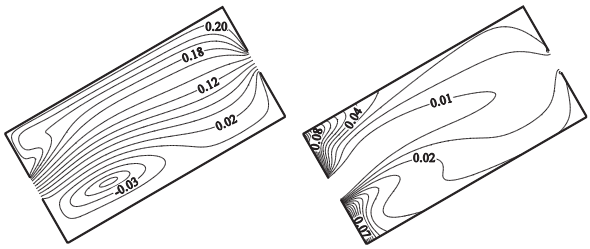

**b)** θ = 30° ($\Psi_{min}$ = -0.042, $\Psi_{max}$ = 0.202

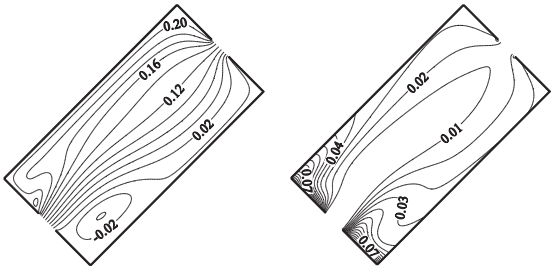

**c)** θ = 45° ($\Psi_{min}$ = -0.036, $\Psi_{max}$ = 0.202)

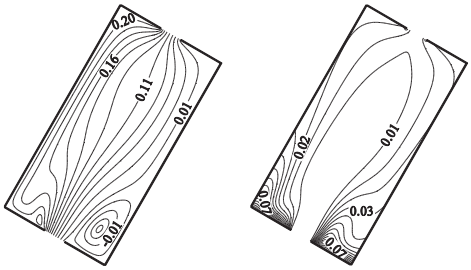

**d)** θ = 60° ($\Psi_{min}$ = -0.031, $\Psi_{max}$ = 0.203)

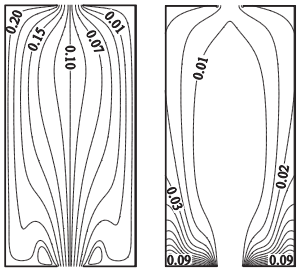

**e)** θ = 90° ($\Psi_{min}$ = -0.004, $\Psi_{max}$ = 0.204)

**Fig. 4.** Flow and thermal fields, in the suction mode, for ε = 0.5, Re = 300 and different cavity inclinations θ

Figure 5 illustrates the variation of the mean convective, radiative, and total Nusselt numbers along the heated wall for Re=300 and two values of surface emissivity (ε = 0.15

and ε = 0.85). Figure 5a shows that for both ventilation modes the convective Nusselt number increases with θ up to about θ ≈ 70°. Beyond this critical angle, the convective contribution becomes almost insensitive to further inclination, except for ε = 0.15 in suction mode, where $Nu_H$(cv) exhibits a non-monotonic behaviour (slight decrease followed by an increase). For a fixed θ, accounting for radiation systematically reduces the convective heat transfer, and this reduction is more pronounced for θ ≤ 70°. Overall, the injection mode provides higher convective performance than the suction mode. Figure 5b shows that the radiative Nusselt number increases markedly with emissivity for both ventilation modes, while it remains practically insensitive to θ and to the choice of injection or suction. The total Nusselt number $Nu_H$, plotted in Figure 5c, exhibits only weak variations with θ for high emissivity values, whereas slight fluctuations are observed at low ε, especially in suction mode. Moreover, the injection mode yields a noticeably higher global heat transfer than the suction mode. For ε = 0.85, switching from suction to injection improves the total heat transfer by about 6.8%, 6.4% and 5% for θ = 0°, 50° and 90°, respectively. For both modes, increasing ε from 0.15 to 0.85 enhances $Nu_H$ by approximately 26.5%, 26.8% and 29.5% at θ = 0°, 50° and 90°, highlighting the strong contribution of radiation.

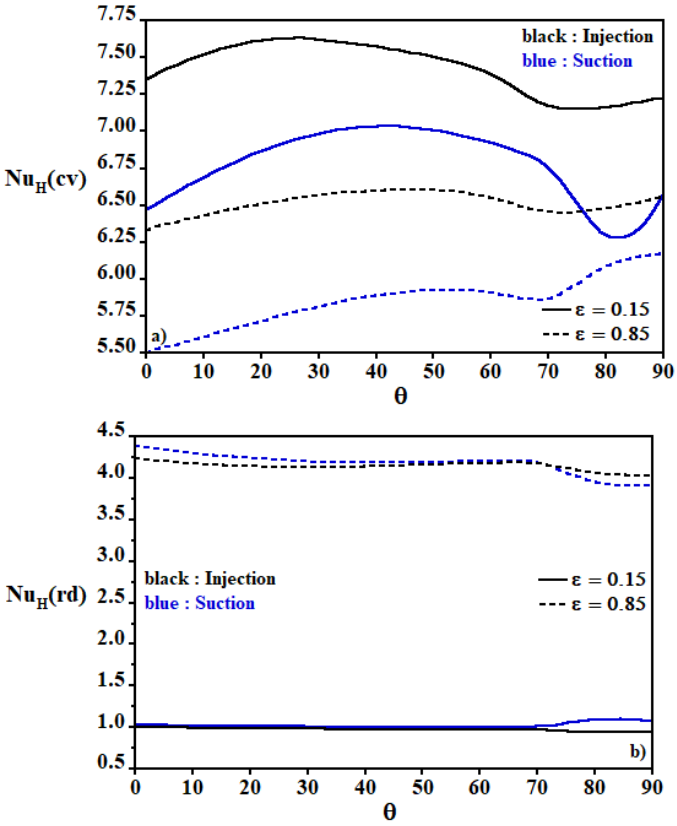

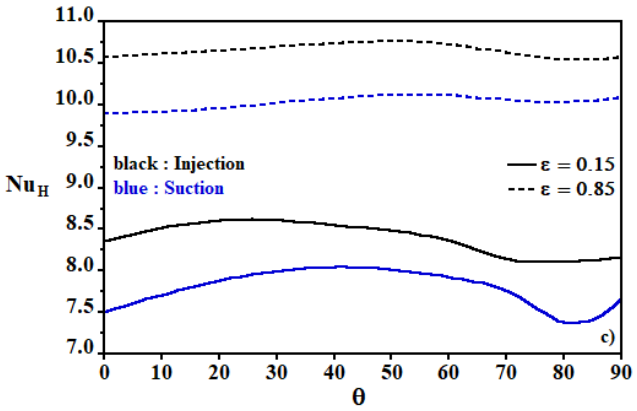


**Fig. 5.** average Nusselt numbers at the heated wall as functions of the inclination angle θ, for various surface emissivities under injection and suction modes : a) $Nu_H(cv)$; b) $Nu_H(rd)$ and c) $Nu_H$

To determine the radiative share of the total heat transfer at the active wall, Figure 6 presents the variation of the ratio $Nu_H(rd) / Nu_H$ as a function of θ for two emissivity values, ε=0.15 and ε=0.85, in both injection and suction modes. The results show that the radiative / (convective) share of the total heat transfer increases / (decreases) with ε over the entire range of inclination angles. Furthermore, the radiative contribution is systematically higher in suction mode than in injection mode and is only weakly influenced by θ. For instance, at θ = 50, the radiative share is about 11.5% / 12.5% for ε = 0.15 and increases to approximately 38.6% / 41.4% for ε = 0.85 in injection / suction mode, respectively, confirming that radiation cannot be neglected even for low walls emissivity.

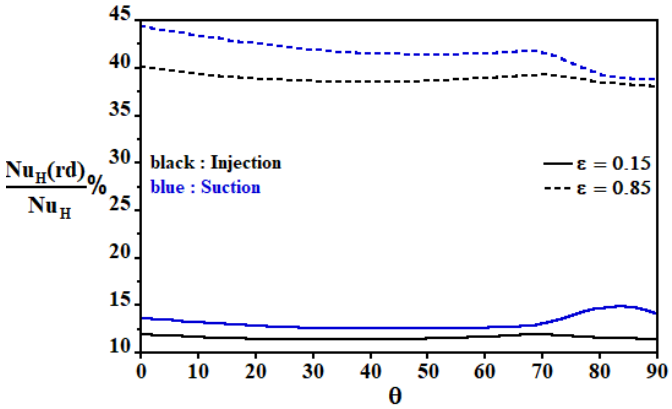


**Fig. 6.** Radiative share of the overall heat transfer at the heated wall versus inclination angle θ, for various values of ε under injection and suction configurations

Figure 7(a) shows the variation of the average temperature inside the cavity as a function of θ for ε = 0.15 and ε = 0.85, in both injection and suction modes. As expected, the mean temperature decreases markedly with increasing inclination angle, reflecting the enhancement of the overall heat removal from the cavity. An exception occurs for ε = 0.15 in suction mode, where a singular behaviour is observed beyond θ ≈ 70: the mean temperature increases slightly. This reheating is consistent with the reduction of the total Nusselt number observed in Figure 5(c) in the same range of θ, and can be attributed to the change in the flow and thermal structures under suction for high inclinations. Overall, the

injection mode yields lower mean temperatures than the suction mode, indicating a more efficient cooling of the cavity.

Figure 7(b) indicates that, for both injection and suction modes, higher emissivity values generally result in a decrease in the maximum temperature $T_{max}$ along the heated wall. For a high emissivity value ($\varepsilon = 0.85$), $T_{max}$ is almost insensitive to the changes of $\theta$ in both injection and suction modes, which indicates that strong radiative exchange helps to stabilise peak wall temperatures. In contrast, for low emissivity, increasing $\theta$ first reduces $T_{max}$, and then leads to a renewed increase for $\theta \gtrsim 70$. This local overheating is linked to the modified flow and thermal fields at high inclination and can be mitigated by enhancing radiation through more emissive walls. It is also worth noting that $T_{max}$ remains higher in suction mode, confirming that injection is more favourable for limiting hot spots on the heated surface.

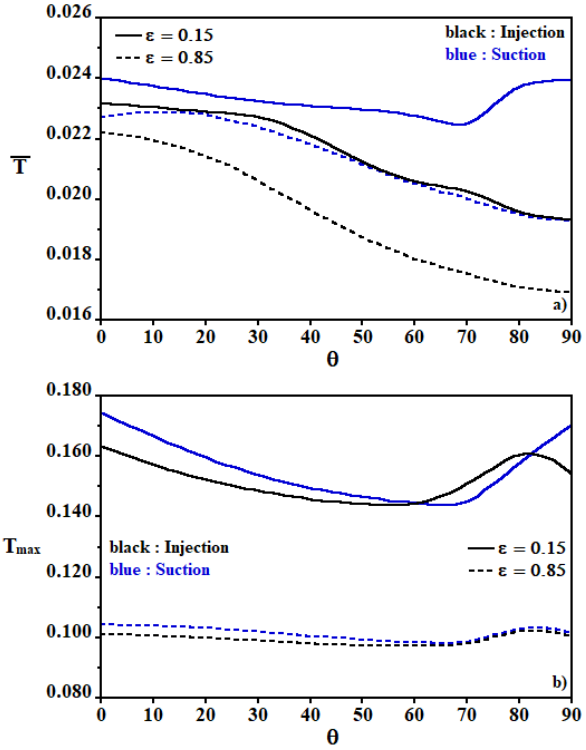


**Fig. 7.** Influence of the inclination angle $\theta$ on the average and peak temperatures for different surface emissivities in suction and injection modes : a) average temperature $\overline{T}$ and b) maximum temperature $T_{max}$

## 4 CONCLUSIONS

In this study, the interaction between mixed convection and surface radiation in an inclined ventilated rectangular cavity was numerically investigated, focusing on the effects of inclination angle, wall emissivity and ventilation mode. The results show that increasing the inclination angle significantly modifies the flow structure and temperature fields which in turn affect both convective and total heat transfer. Higher wall emissivity enhances the radiative share of the heat flux and contributes to a marked decrease in maximum wall temperature, even for moderate inclination angles. The radiative contribution remains significant over the entire range of studied parameters and cannot be neglected, even for

low emissivity values. It is slightly more pronounced in suction mode, whereas injection generally provides better overall cooling and lower peak temperatures.These outcomes underline the importance of jointly optimizing inclination and ventilation strategy to improve the thermal performance of ventilated enclosures where convection and radiation are strongly coupled.

Nomenclature

| | |
|---|---|
| $t$ | dimensionless time $(= t'u_o'/H')$ |
| $L'$ | enclosure width (m) |
| $H'$ | enclosure height (m) |
| $A$ | shape ratio of the enclosure $(= L'/H')$ |
| $h$ | relative opening height $(= h'/H')$ |
| $(x, y)$ | dimensionless coordinates $(= (x', y')/H')$ |
| $(u, v)$ | dimensionless horizontal and vertical velocities $(= (u', v')/H')$ |
| $u_o'$ | inlet flow velocity $(m/s)$ |
| $T'$ | dimensional fluid temperature (K) |
| $T_c'$ | inlet air temperature (K) |
| $T$ | dimensionless fluid temperature $(= \lambda(T' - T_c')/q'H')$ |
| $\overline{T}$ | dimensionless mean temperature |
| $F_{ij}$ | view factor between surface elements $S_i$ and $S_j$ |
| $Q_r$ | nondimensional net radiative heat flux $\left(= Q_r'/\sigma {T_c'}^4\right)$ |
| $q'$ | heat flux applied to the active wall $(W/m^2)$ |
| $I_i$ | dimensionless irradiation $\left(= I_i'/\sigma {T_c'}^4\right)$ |
| $J_i$ | dimensionless radiosity $\left(= J_i'/\sigma {T_c'}^4\right)$ |
| $N_r$ | radiation–convection coupling number $\left(= \sigma {T_c'}^4/q'\right)$ |
| $Ri$ | Richardson number $(= Ra/Re^2Pr)$ |
| $T_o$ | dimensionless reference temperature $(= \lambda T_c'/q'H')$ |
| $Re$ | Reynolds number $(= u_o'H'/\nu)\left(= u_o'H'/\nu\right)$ |
| $Pr$ | Prandtl number $(= \nu/\alpha)$ |
| $Nu$ | average Nusselt number |
| $Ra$ | Rayleigh number $\left(= g\beta q'{H'}^4/\alpha\nu\lambda\right)$ |

Greek symbols

| | |
|---|---|
| $\sigma$ | Stéfan-Boltzman constant $(= 5.67 \times 10^{-8}\, W/m^2K^4)$ |
| $\Psi$ | dimensionless stream function $(= \Psi'/u_o'H')$ |
| $\Omega$ | dimensionless vorticity $(= \Omega' H'/u_o)$ |
| $\alpha$ | fluid thermal diffusivity $(m^2/s)$ |
| $\beta$ | fluid thermal expansion coefficient $(1/K)$ |
| $\varepsilon$ | surface emissivity of the walls |
| $\lambda$ | fluid thermal conductivity $(W/(K.m))$ |
| $\nu$ | fluid kinematic viscosity $(m^2/s)$ |

Subscripts

| | | | |
|---|---|---|---|
| C | cold | max | maximum value |
| H | hot | min | minimum value |

Superscripts

′ dimensional variable

## References

1. M. Bouafia, S. Hamimid, M. Guellal, Non-Boussinesq convection in a square cavity with surface thermal radiation. Int. J. Therm. Sci. **96**, 236–247 (2015).
2. [X] M. Ali, A.K. Sharma, Numerical simulation of combined natural convection and radiation inside a square enclosure with a horizontal partition, in Fluid Mechanics and Fluid Power, Lect. Notes Mech. Eng. **3**, Springer, 329–337 (2024).
3. H. Karatas, T. Derbentli, Natural convection and radiation in rectangular cavities with one active vertical wall. Int. J. Therm. Sci. **123**, 129–139 (2018).
4. S. Yang, L. Li, B. Wang, Y. Zheng, P. Lund, J. Wang, Y. Ding, Modelling of radiative and convective heat transfer in an open cavity volumetric receiver for a 50-MWth integrated beam-down receiver-storage concentrating solar thermal system. Renew. Energy **242**, 122457 (2025).
5. A. Daiz, A. Bahlaoui, I. Arroub, S. Belhouideg, A. Raji, M. Hasnaoui, Simulation of combined thermal mixed convection and radiation in a discretely heated lid-driven cavity using a lattice Boltzmann method. Advances in Mechanics, Lect. Notes Mech. Eng., Springer, 191–200 (2023).
6. R. Hidki, L. El Moutaouakil, M. Boukendil, Z. Charqui, B. Jamal, Analysis of mixed convection and surface radiation in a horizontal channel containing different finned heat-generating blocks. Therm. Sci. Eng. Prog. **48**, 102370 (2024).
7. R. Ganesan, A.N. Sung, K. Perumal, S.Y.H. Onn, M. Rajayokkiam, Numerical investigation of combined convection and radiation heat transfer in the horizontal ducts heated from different orientations, AIP Conf. Proc. 2676, 050005 (2022).
8. Y. Dahani, M. Hasnaoui, A. Amahmid, A. El Mansouri, S. Hasnaoui, Lattice Boltzmann simulation of combined effects of radiation and mixed convection in a lid-driven cavity with cooling and heating by sinusoidal temperature profiles on one side. Heat Transfer Eng. **41**, 433–443 (2019).
9. O. Prakash, S.N. Singh, Experimental and numerical study of mixed convection with surface radiation heat transfer in an air-filled ventilated cavity. Int. J. Therm. Sci.**171**, 107169 (2022).
10. Prakash, S.N. Singh, Study of mixed convection with surface radiation in a ventilated cavity with uniform heat generating source, Proceedings of the 25th National and 3rd International ISHMT-ASTFE Heat and Mass Transfer Conference, Roorkee, India, 2688–7231 (2019)
11. M. Raji, M. Hasnaoui, Combined mixed convection and radiation in ventilated cavities. Eng. Comput. **18**, 922–949 (2001).
12. A. Bahlaoui, A. Raji, M. Hasnaoui, M. Naïmi, T. Makayssi, M. Lamsaadi, Mixed convection cooling combined with surface radiation in a partitioned rectangular cavity. Energy Convers. Manag. **50**, 626–635 (2009).
13. L.C. Woods, on compressible boundary layers. Aero. Quart. **5**, 176–184 (1954).

14. H.C. Hottel, A.F. Saroffim, Radiative Heat Transfer (McGraw-Hill, New York, 1967).
15. H. Wang, S. Xin, P. Le Quéré, Étude numérique du couplage de la convection naturelle avec le rayonnement de surfaces en cavité carrée remplie d'air. C. R. Mécanique **334**, 48–57 (2006).